Resonant Circular Dichroism of Chiral Metal-Organic Complex

D. Catone,[1] M. Stener,[2,3,4,*] P. Decleva,[2,3,4] G. Contini,[1] N. Zema,[1] T. Prosperi,[1] V. Feyer,[5] K. C. Prince,[5,6] and S. Turchini[1]

[1]*Istituto Struttura della Materia, C.N.R. Via Del Fosso del Cavaliere 100, 00133 Roma, Italy*
[2]*Dipartimento di Scienze Chimiche e Farmaceutiche, Università di Trieste, Via Licio Giorgieri 1, I-34127 Trieste, Italy*
[3]*Consorzio Interuniversitario Nazionale per la Scienza e Tecnologia dei Materiali, INSTM, Unitá di Trieste, Trieste, Italy*
[4]*DEMOCRITOS CNR-IOM National Simulation Center, Trieste, Italy*
[5]*Sincrotrone Trieste, I-34149 Basovizza, Trieste, Italy*
[6]*IOM-CNR, I-34149, Basovizza, Trieste, Italy*

(Received 8 August 2011; published 23 February 2012)

A sizable enhancement of the circular dichroism in photoelectron spectroscopy has been measured and computed for the metal complex Δ-cobalt(III) *tris*-acetylacetonate highest occupied molecular orbital state in the region of the Co $3p \rightarrow 3d$ Fano resonance. In the resonance the dichroism reaches the maximum value of 5% and even changes its sign as compared to the direct photoionization channel. We ascribe this enhancement to electron correlation processes, namely, with the coupling between discrete excitations and the continuum, which is correctly described in the time dependent density functional theory (TDDFT) framework. These findings open new physical aspects of photoelectron circular dichroism that now can be interpreted not only via the simple direct ionization, but also through more complex electron correlation processes.

DOI: 10.1103/PhysRevLett.108.083001 PACS numbers: 33.80.Eh

Absorption circular dichroism, describing the different transition probabilities between right and left circularly polarized light excitations experienced by chiral molecules, is a well known physical phenomenon, widely used to investigate structural and optical properties of dissymmetric systems [1]. The measured experimental difference in the total absorption originates for unoriented molecules from the second order electric dipole-magnetic dipole $E1$-$M1$ term and therefore a rather weak effect of the order of 10^{-3}–10^{-4} is typically expected and observed. In 1976 Ritchie [2] and later Cherepkov [3] showed theoretically the appearing in angular resolved photoelectron spectroscopy of dichroism at electric dipole level ($E1$); for this reason the expected signal in this process is stronger than in absorption with an intensity of the order of 10^{-2}. Circular dichroism in the angular distribution of photoelectrons is a well-established technique used to analyze structural properties of oriented and ordered surface-interface systems [4,5]. Although the effect was already predicted since 1976, only in the last decade has the photoelectron circular dichroism (PECD) effect been experimentally investigated to study structural and electronic properties of unoriented chiral molecules in the gas phase, receiving increasing attention [6,7]. The PECD can be formulated for each ith electronic state of the molecular system in terms of the differential cross section $\frac{d\sigma_i}{d\hat{k}}$ [8], representing the flux of photoelectrons in the solid angle $d\hat{k}$ along the direction of propagation $\hat{k}$, and is completely described by three dynamical quantities, namely, the cross section σ_i, the asymmetry parameter β_i, and the dichroism parameter D_i:

$$\frac{d\sigma_i}{d\hat{k}} = \frac{\sigma_i}{4\pi}[1 + (-1/2)^{|m_r|}\beta_i P_2(\cos\theta) + m_r D_i P_1(\cos\theta)], \quad (1)$$

where P_j is the Legendre polynomial of jth order, θ is the scattering angle between $\hat{k}$ and the laboratory frame, m_r is 0, +1 or −1 for linear, left circular or right circular polarization, respectively. The laboratory frame is defined by the incident photons: the polar axis corresponds to the electric vector or propagation direction for linear or circular light polarization, respectively. The third term in (1) is the dichroic term. It is nonzero only for chiral molecules and changes sign exchanging the enantiomers [9]. The β contribution is eliminated measuring the D parameter at a fixed magic scattering angle (54.7°), for which $P_2(\cos\theta) = 0$.

The PECD can be completely described by the dependence of the dichroic parameter D_i of Eq. (1) with respect to the photoelectron kinetic energy. In previous theoretical and experimental studies on PECD, it has been found that the dichroic parameter D usually does not exceed a few percent of the photoelectron intensity and shows the most prominent spectral features within the first 30 eV above the ionization threshold [10–12].

The most common resonant behaviors are represented by the shape resonances and the Feshbach autoionization resonances. Occasionally autoionization resonances can become extremely intense (''giant resonances'') and this happens, for example, when a discrete transition is strongly coupled with transitions to the continuum, as in the case of the $3p \rightarrow 3d$ excitation in transition metal atoms [13–15], such transitions are very intense since they take place

between atomic functions belonging to the same shell, with principal quantum number $n = 3$. For molecules, an example of strong autoionization resonance is the Cr $3p \rightarrow 3d$ transition in $Cr(CO)_6$ (band A), studied experimentally [16] and theoretically [17].

We focused our investigation on Δ-cobalt(III) *tris*-acetylacetonate [$Co(acac)_3$], which is a very convenient model compound for chiral metal complexes, due to its high symmetry (D_3 point group) which allows an easier interpretation of the results and makes computations cheaper, to its closed shell electronic structure and to the availability of efficient asymmetric synthesis.

In the case of $Co(acac)_3$, in correspondence of the autoionization resonance, the very intense discrete Co $3p \rightarrow 3d$ transition is coupled with the highest occupied molecular orbital (HOMO) direct ionization and the dichroic dispersion of the specific D_i provides new insights into the electronic excitations in chiral molecules.

The PECD measurements of the $Co(acac)_3$ molecule were performed at the 4.2 circular polarization beam line at Elettra Synchrotron Radiation Facility (Trieste, Italy), equipped with a grazing incident spherical grating monochromator (SGM) and a normal incidence monochromator (NIM) sharing the same entrance and exit slits [18]. The photoelectron spectra were recorded using a VG, 6-channel, 150 mm hemispherical electron energy analyzer, placed at 54.7° with respect to the synchrotron radiation polarization vector. The analyzer was set at 20 eV pass energy and the overall resolution was about 200 meV. In this work the exploited excitation energy range was 15–32 eV with a variable polarization ratio from 60% to 80% and 50–70 eV with polarization ratio 95% at the Co $3p$ resonance. The complete enantiomeric resolution of $Co(acac)_3$ was achieved by following the recipe reported in the literature [19]. The $Co(acac)_3$ was evaporated from a noncommercial, noninductively wound furnace, whose temperature was kept constant at about 100 °C. The pressure in the chamber was 6×10^{-6} mbar (base pressure 8×10^{-7} mbar). In order to improve the experimental accuracy and the signal to noise ratio of D parameter, PECD measurements were taken reversing the helicity at 0.05 Hz frequency, allowing us to measure the two helicity branch of the spectrum at each kinetic energy point. The complete methodology for experimental D extraction and analysis, including the correction for the ellipticity of light, is described elsewhere [11]. The HOMO constant initial state (CIS) photoemission intensity measurements were obtained by fitting photoelectron spectra.

The calculation of the autoionizing resonant PECD is challenging for theory, since it requires the explicit treatment of the electron continuum as well as the inclusion of the interchannel mixing, in order to allow the coupling between the discrete transition and the ionization. This was recently achieved by implementing the linear combination of atomic orbitals (LCAO) B-spline method [20] in the framework of the time dependent density functional theory (TDDFT). The LCAO B-spline functions are suitable to manage the oscillatory behavior of the continuum boundary conditions, while TDDFT allows interchannel coupling. The LB94 exchange-correlation potential was employed [21], while the B-spline functions centered on the center of mass of the molecule (the Co atom) were expanded up to an angular momentum $L = 20$, for off-center nuclei the angular momentum expansion has been limited to $L = 2$ for C and O and to $L = 1$ for H. To calculate the PECD, conventional expressions for the D_i terms were developed [9], while the transition moments were generated by using Φ^{SCF} potential obtained solving the TDDFT equation [20] instead of the dipole operator [17]. All TDDFT calculated profiles have been convoluted by Gaussian functions with FWHM = 1 eV in order to smooth the many narrow autoionization resonances which show up at low kinetic energies. The ground state electronic structure of $Co(acac)_3$ [22], used as input for the TDDFT B-spline calculation [20], was obtained at the Kohn-Sham (KS) level, using DZP STO basis set and LB94 exchange-correlation potential [21] employing the ADF program [23,24]. The molecular orbitals of $Co(acac)_3$ were conveniently described as being formed by different fragments, i.e., three acetylacetonate moieties (the ligands *acac*) and the central Co atom, as reported in Fig. 1. The ligand orbitals relevant for the chemical bonds are two lone pairs (LP+ and LP- designate a linear combination with the same or opposite sign of the LP, respectively) on the two carbonylic oxygens which lie on the plane containing the C and O atoms of the ligand, and the 3π orbital which is perpendicular to the same plane. The electronic structure of the complex can be then obtained allowing the interaction among three ligand units $(acac)_3$ and finally setting the Co atom in the center. The D_3 symmetry of this site removes the five Co $3d$ atomic orbitals degeneracy and splits them into the $e + e + a_1$ irreducible representations mixing with ligand orbitals. More precisely the $30e$ orbital (HOMO) consists of a pair of Co $3d$ atomic functions

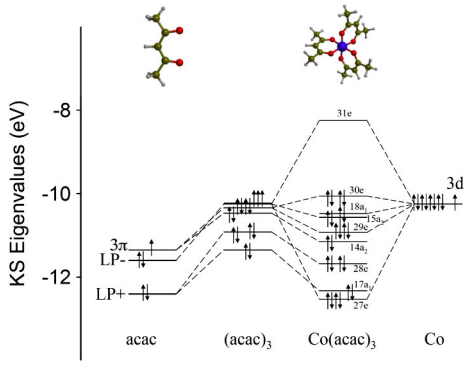

FIG. 1 (color online). Schematical representation of the molecular orbitals energy levels of ground state electronic structure of $Co(acac)_3$ and its fragments.

slightly destabilized by antibonding interaction with 3π ligand wave functions, and the virtual $31e$ orbital (lowest occupied molecular orbital—LUMO) consists of a pair of Co $3d$ functions strongly destabilized by σ antibonding interaction with ligand LPs. Clear assignment of the bands appearing in the experimental photoelectron spectrum [22] to the electronic states at higher binding energies than HOMO is rather complicated due to their strong overlapping, as reported in Fig. 1. In this Letter we focused our analysis to the HOMO, safely assigned to the photoelectron K band (see inset of Fig. 3), that presents an almost pure Co $3d$ electronic character.

The calculated dispersion, by using both KS (gray line) and TDDFT (black line) computational methods, of cross section σ, asymmetry parameter β, and dichroism parameter D of Co$(acac)_3$ HOMO, are reported in Fig. 2. The HOMO ionization cross section (upper panel of Fig. 2) displays a strong and sharp feature at 5 eV of kinetic energy, followed by a lower maximum at about 18 eV. These two features, present in both TDDFT and KS curves, were assigned to shape resonances. Above 50 eV a prominent structure appears only in the TDDFT curve, displaying a typical Fano profile. This feature is ascribed to an interchannel interference effect (Feshbach resonance), which results from the autoionizing coupling between the direct ionization of the HOMO and the excitation of the discrete transition Co $3p \rightarrow$ LUMO. The comparison between KS and TDDFT is informative, since features which appear in the TDDFT profiles are ascribed to autoionizations since interchannel coupling is present in TDDFT scheme while it is missing in KS formalism. In the central panel of Fig. 2 the calculated asymmetry parameter β for HOMO is reported. The structures at low kinetic energy are less evident than in the cross section, but at about 55 eV a prominent feature appears only in the TDDFT profile, in the same energy range of the autoionization resonance. The dichroic parameter, calculated at KS and TDDFT level of theory and reported in the lower panel of Fig. 2, presents two prominent structures of comparable intensity at low kinetic energy (9 and 17 eV, respectively). Above 35 eV the dichroism predicted by KS theory remains very close to zero, while the TDDFT shows a pronounced negative oscillation in correspondence to the autoionization resonance. This particular behavior points out how the calculated PECD resulting in the electron correlation regime can be significantly different from the one obtained taking into account only the direct photoionization process, well represented by the KS prediction. Figures 3 and 4 compares the present experimental data with the TDDFT profiles, all these latter have been sifted by +2.84 eV. This shift has been done since it is known that calculated profiles tend to be systematically moved to lower energy, due to overestimation of the attractive nature of the LB94 exchange-correlation potential employed in the calculations. The value of the energetic shift corresponds to the difference between the experimental IE and the opposite of the KS eigenvalue of the HOMO.

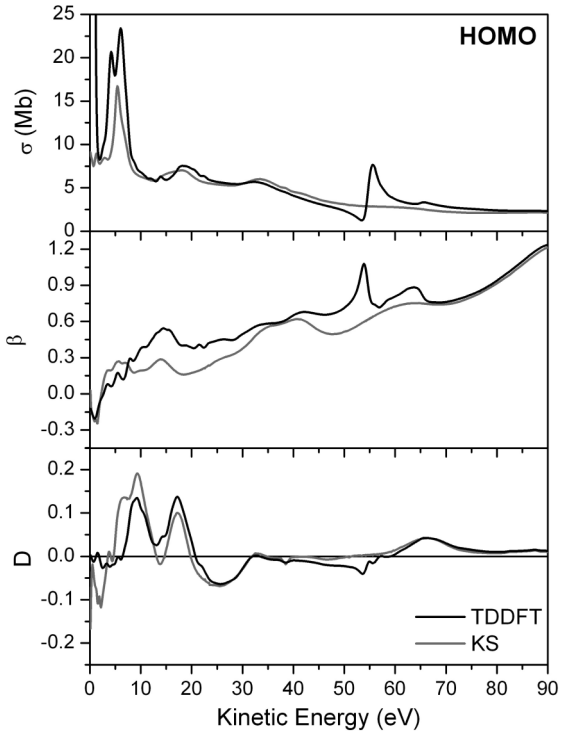

FIG. 2. Calculated cross section σ (upper panel), asymmetry parameter β (central panel), and dichroic parameter D (lower panel) of Co$(acac)_3$ HOMO. Kohn-Sham (KS) profile, gray line; time dependent density functional theory (TDDFT) profile, black line.

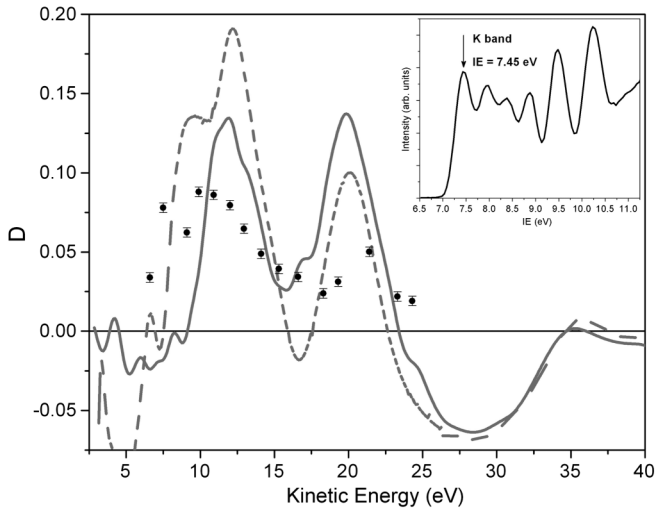

FIG. 3. Experimental dichroic dispersion (black dots), TDDFT calculated D profile (solid gray line), and KS calculated D profile (dashed gray line) in off-resonance region. Inset: photoelectron spectrum of Co$(acac)_3$, acquired at 29 eV of photon energy; the arrow highlights the K band (HOMO) at IE of 7.45 eV.

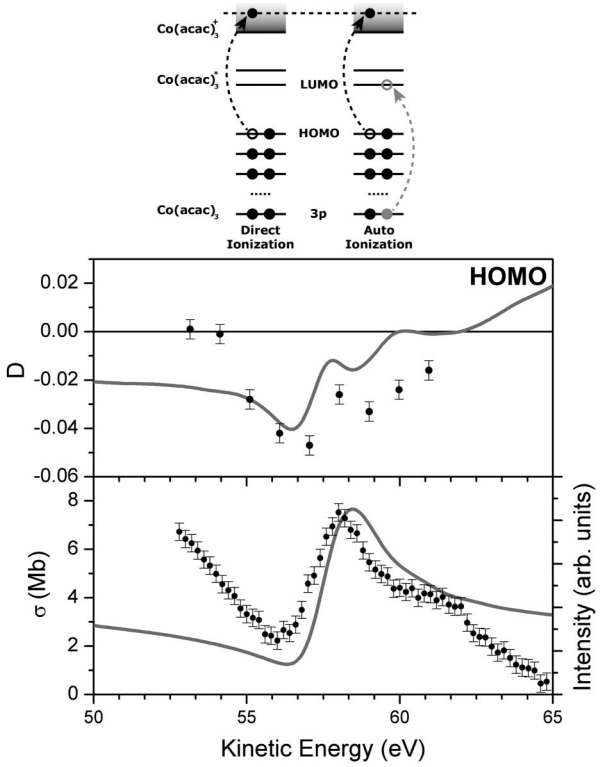

FIG. 4. Upper panel: schematic representation of direct ionization and autoionization processes for HOMO state. Central panel: experimental dichroic dispersion (black dots) and TDDFT calculated D profile (gray line) in the Co $3p \rightarrow 3d$ autoionization resonance region. Lower panel: experimental HOMO photoemission intensity (black dots) and TDDFT calculated cross section (gray line) in the Co $3p \rightarrow 3d$ autoionization resonance region.

Figure 3 reports the experimental D values for Co$(acac)_3$ HOMO taken in the 5–25 eV kinetic energy range together with the calculated KS (dashed gray line) and TDDFT (solid gray line) curve. The photoelectron valence state spectrum of Co$(acac)_3$, acquired at 29 eV of exciting photon energy, is reported in the inset of Fig. 3, highlighting the K band (HOMO) position at 7.45 eV IE . The experimental data present a double peak structure that is well reproduced by the TDDFT profile, even if the theory predicts two peaks with higher intensity and narrower shape with respect to what is experimentally obtained. This discrepancy is probably caused by the thermal motions of the molecules, which theory assumes frozen at the equilibrium distances in a fixed geometry, but actually are subjected to vibrations, even of large amplitude, as well as free rotation of the methyl groups of the ligands [25,26]. Below 10 eV the theory predicts a slightly negative dichroism although the experimental findings remain positive; this disagreement is probably related to electron correlation, which plays a more and more important role approaching the ionization threshold but is only partially accounted for in the TDDFT formalism. The oscillation shape, the intensity, and the sign are very similar in the both KS and TDDFT predictions, and the small differences between them cannot be sufficient to assign a preferential agreement with the experimental data. For this reason we can conclude that the experimental D is reproduced with the same qualitative level by both theoretical methods, meaning that in this energy region, far from an autoionization resonance, direct ionization dominates the electronic processes involved in the dichroic description.

The processes of direct ionization and autoionization are schematically reported in the upper panel of Fig. 4, that shows how the final ionic state $Co(acac)_3^+$ can be reached via two different channels: the direct ionization, or the two-step process, which starts with a discrete excitation transition involving a Co $3p$ electron promoted in LUMO and ends with an autoionization. The quantum interference between these two processes gives rise to the typical Fano shape resonance. The measured HOMO CIS photoemission intensity is reported in the lower panel of Fig. 4, together with the cross section predicted by TDDFT, in the 50–65 eV kinetic energy range. The experimental data show a clear Fano profile very well reproduced at the TDDFT level, so the latter proves to be very sensitive to the coupling matrix elements between the discrete excitation and the ionization to continuum. We observe some disagreements between TDDFT prediction and experimental data. In particular before the resonance the signal slope is much more pronounced than in the predicted curve, and this is likely ascribed to nonquantifiable contributions in the normalization procedure, due to monochromator higher orders recorded by the photodiode. On the other hand around 62 eV a weak feature is apparent in the experiment but missing in the calculated profile, this is probably due to a many-body effect not included in the present theory.

The experimental dichroism of HOMO in the region of the Co $3p \rightarrow$ LUMO autoionization resonance is reported in the central panel of Fig. 4, together with the TDDFT curve. The agreement between theory and experiment is very satisfactory, since the calculation correctly reproduces the experimental data in intensity and shape. Below 55 eV the experimental D is almost zero while the TDDFT profile remains slightly negative. We do not expect a deterioration of the method in the off-resonance region, but it should be considered that the formalism includes only channel coupling between one-electron excited configurations, so higher order many-body effects are neglected. At the autoionization resonance the experimental dichroism comes up to 5%, while at 60 eV KS predictions are very close to zero. The sign of dichroism is opposite with respect to the low kinetic energy region characterized by direct ionization of the valence states, indicating a different influence of the absorption process promoting electrons in the continuum and autoionization mediated electron emission.

In conclusion, the experimentally detected enhancement in the photoelectron dichroism for the Co$(acac)_3$ HOMO

state in correspondence of the Co $3p \rightarrow 3d$ autoionization resonance region has been ascribed to electron correlation processes, since the presented computational scheme correctly describes the coupling between the discrete excitation and the continuum, shedding light on new physical aspects of PECD that now can be interpreted not only via the simple direct ionization, but also through the more complex electron correlation processes. Moreover, the satisfactory agreement between theory and experiment in the off-resonance energy region proves that the calculation method can also account for the structural and electronic sensitivity of PECD in such metal-organic complex in direct ionization regime. The TDDFT approach has been demonstrated to be suitable for correlated electronic description such as experimental quantitative studies of resonant PECD of chiral metal-organic systems, opening the way for systematic characterization of transition metal contribution in metallorganic complexes. These studies will open new opportunities for investigating biochemical chiral systems, such as enzymes whose enantioselectivity is determined by the electronic interaction between the central metal ion and the surrounding biomolecules.

This work has been supported by grants from MIUR Programmi di Ricerca di Interesse Nazionale (PRIN) of Italy. A generous CINECA ISCRA B HP10BFIMTY grant for computer time on the IBM SP6 of CINECA (Bologna, Italy) is gratefully acknowledged. We thank the Elettra staff for providing good quality synchrotron radiation and Mr. Sandro Rinaldi for his valuable technical assistance in setting up the experimental apparatus. Thanks are due also to Dr. F. Cattaruzza for the resolution of the racemic Co$(acac)_3$ molecule.

*Corresponding author.
stener@univ.trieste.it

[1] L. Barron, *Molecular Light Scattering and Optical Activity* (Cambridge University Press, Cambridge, U.K., 2004).
[2] B. Ritchie, Phys. Rev. A **13**, 1411 (1976).
[3] N. A. Cherepkov, Chem. Phys. Lett. **87**, 344 (1982).
[4] C. Westphal, J. Bansmann, M. Getzlaff, and G. Schönhense, Phys. Rev. Lett. **63**, 151 (1989).
[5] G. Schönhense, Phys. Scr. **T31**, 255 (1990).
[6] N. Böwering, T. Lischke, B. Schmidtke, N. Müller, T. Khalil, and U. Heinzmann, Phys. Rev. Lett. **86**, 1187 (2001).
[7] G. A. Garcia, L. Nahon, M. Lebech, J. C. Houver, D. Dowek, and I. Powis, J. Chem. Phys. **119** 8781 (2003).
[8] N. Chandra, J. Phys. B **20**, 3405 (1987).
[9] M. Stener, G. Fronzoni, D. Di Tommaso, and P. Decleva, J. Chem. Phys. **120**, 3284 (2004).
[10] S. Stranges, S. Turchini, M. Alagia, G. Alberti, G. Contini, P. Decleva, G. Fronzoni, M. Stener, N. Zema, and T. Prosperi, J. Chem. Phys. **122**, 244303 (2005).
[11] S. Turchini, D. Catone, G. Contini, N. Zema, S. Irrera, M. Stener, D. Di Tommaso, P. Decleva, and T. Prosperi, Chem. Phys. Chem. **10**, 1839 (2009).
[12] A. Giardini, D. Catone, S. Stranges, M. Satta, M. Tacconi, S. Piccirillo, S. Turchini, N. Zema, G. Contini, T. Prosperi, P. Decleva, D. Di Tommaso, G. Fronzoni, M. Stener, A. Filippi, and M. Speranza, Chem. Phys. Chem. **6**, 1164 (2005).
[13] R. Bruhn, B. Sonntag, and H. W. Wolff, J. Phys. B **12**, 203 (1979).
[14] E. Schmidt, H. Schroder, B. Sonntag, H. Voss, and H. E. Wetzel, J. Phys. B **16**, 2961 (1983).
[15] L. C. Davis and L. A. Feldkamp, Phys. Rev. B **23**, 6239 (1981).
[16] G. Cooper, J. C. Green, M. P. Payne, B. R. Dobson, and I. H. Hillier, J. Am. Chem. Soc. **109**, 3836 (1987).
[17] M. Stener, G. Fronzoni, and P. Decleva, Chem. Phys. **361**, 49 (2009).
[18] A. Derossi, F. Lama, M. Piacentini, T. Prosperi, and N. Zema, Rev. Sci. Instrum. **66**, 1718 (1995).
[19] A. F. Drake, J. M. Gould, S. F. Mason, C. Rosini, F. J. Woodley, Polyhedron **2**, 537 (1983).
[20] M. Stener, G. Fronzoni, and P. Decleva, J. Chem. Phys. **122**, 234301 (2005).
[21] R. van Leeuwen and E. J. Baerends, Phys. Rev. A **49**, 2421 (1994).
[22] S. Evans, A. Hamnett, A. F.Orchard, and D. R. Lloyd, Faraday Discuss. Chem. Soc. **54**, 227 (1972).
[23] E. J. Baerends, D. E. Ellis, and P. Ros, Chem. Phys. **2**, 41 (1973).
[24] C. Fonseca Guerra, J. G. Snijders, G. te Velde, and E. J. Baerends, Theor. Chem. Acc. **99**, 391 (1998).
[25] Devis Di Tommaso, M. Stener, G. Fronzoni, and P. Decleva, Chem. Phys. Chem. **7**, 924 (2006).
[26] G. Contini, N. Zema, S. Turchini, D. Catone, T. Prosperi, V. Carravetta, P. Bolognesi, L. Avaldi, and V. Feyer, J. Chem. Phys. **127**, 124310 (2007).